

Numerical Analysis on Mixed Convection Flow in a Lid-Driven Triangular Cavity

Mohammed Nasir Uddin^{1*}, M.N.Huda², Aki Farhana³, M.A.Alim⁴

¹Department of Information & Communication Technology (ICT), Bangladesh University of Professionals (BUP), Bangladesh.

²Wing Commander, Deputy Director of Education, Air Headquarters, Bangladesh.

³Department of Mathematics, Nanyang Technological University (NTU), Singapore

⁴Department of Mathematics, Bangladesh University of Engineering & Technology (BUET), Bangladesh

Abstract: In the present paper, the effect of dimensionless parameter on mixed convection flow within a lid-driven triangular cavity has been numerically investigated. The bottom wall of the cavity is considered as heated. Besides, the left and the inclined wall of the triangular cavity are assumed to be cool and adiabatic respectively. The cooled wall of the cavity is moving up in the vertical direction. The developed mathematical model is governed by the coupled equations of continuity, momentum and energy to determine the fluid flow and heat transfer characteristics in the cavity as a function of Rayleigh number, Prandtl number and the cavity aspect ratio. The proposed numerical procedure adopted in this investigation yields consistent performance over a wide range of parameters such as Rayleigh number Ra (10^3 - 10^4), Prandtl number Pr (0.71 – 6.00) and cavity aspect ratio (0.5 – 1.5). The numerical results have been presented in terms of stream functions, temperature profile and Nusselt numbers. It is found that the streamlines, isotherms, average Nusselt number and average fluid temperature in the cavity strongly depend on Rayleigh number, Prandtl number and cavity aspect ratio.

Keywords: Finite element method, Lid-driven triangular cavity, mixed convection, Prandtl number, Rayleigh number

Nomenclature

CAR	Cavity aspect ration	T	Temperature (K)
Gr	Grashof number	ΔT	Temperature difference
Re	Reynolds number	V_0	Lid velocity (ms^{-1})
Ra	Rayleigh number	C_p	Specific heat at constant pressure (J/kg K)
Pr	Prandtl number, ν/α	x, y	Cartesian coordinates (m)
Nu	Average Nusselt number	X, Y	Non-dimensional Cartesian coordinates
g	Gravitational acceleration (ms^{-2})	u, v	Velocity components (ms^{-1})
k	Thermal conductivity of the fluid ($\text{Wm}^{-1}\text{K}^{-1}$)	U, V	Non-dimensional velocity components
h	Convective heat transfer coefficient (W/m^2)	Greek symbols	
K)		α	thermal diffusivity, (m^2s^{-1})
N	Non-dimensional distance	β	thermal expansion coefficient (K^{-1})
\bar{V}	Cavity volume	θ	Fluid temperature
L	Height of the cavity	ρ	density of the fluid (kgm^{-3})
p	Pressure (Nm^{-2})	ν	kinematic viscosity of the fluid (m^2s^{-1})
P	Non-dimensional pressure	Subscripts	
q	Heat flux (Wm^{-2})	P	constant pressure
T_c	Temperature of cold wall (K)	av	average
T_h	Temperature of hot wall(K)	h	hot
θ	Dimensional temperature	c	cold
θ_{av}	Average temperature		

I. Introduction

Mixed convection phenomenon occurs in many engineering systems such as cooling of electronic devices, drying technology, solar collectors, flat glass manufacturing, nuclear reactors etc. The cavity with moving lid is the most important application for these heat transfer mechanisms, which is seen in cooling of electronic chips, solar energy collection, food industry etc. Numerical analysis of these kinds of systems can be found in many literatures. Akinsete and coleman [1] first studied the various flow system in triangular cavity. They solved the problem for various aspect ratios and Grashof numbers (Gr) and concluded that heat transfer across the base wall increase towards the hypotenuse and base intersection. Karyakin and Sokovishin [9]

presented convection patterns in isosceles triangular enclosure. M. Li and T. Tang [13] studied the steady viscous flow in a triangular cavity by efficient numerical techniques. They found accurate and efficient calculations of the flow inside a triangular cavity are presented for high Ra numbers. Moallemi and Jang [14] investigated mixed convective flow in a bottom heated square lid-driven cavity. The authors studied the effect of Prandtl number on the flow and heat transfer process. They found that the effects of buoyancy are more pronounced for higher values of Prandtl number, and also derived a correlation for the average Nusselt number in terms of the Prandtl number, Reynolds number and Richardson number. Prasad and Koseff [16] experimentally investigated mixed convection heat transfer in deep lid-driven cavities heated from below. The authors observed that the heat transfer was rather insensitive to the Richardson number. Later on, Aydin and Yang [2] numerically studied mixed convection heat transfer in a two-dimensional square cavity having an aspect ratio of 1. In their configuration, the isothermal sidewalls of the cavity were moving downwards with uniform velocity while the top wall was adiabatic. Oztop and Dagtekin [15] investigated numerically steady-state two-dimensional mixed convection problem in a vertical two-sided lid-driven differentially heated square cavity. Hossain and Gorla [7] observed the effects of viscous dissipation on unsteady combined convective heat transfer to water near its maximum density in a rectangular cavity with isothermal wall. Luo and Yang [12] numerically found two-dimensional flow in a two-sided lid-driven cavity containing a temperature gradient. Analysis of the cavity phenomena incorporating a solid material extends its usability in the engineering fields. Considering the complexity of phenomenon in side an obstructed cavity with moving wall, a brief review on the relevant literature has been hereby presented. Roychowdhury et al. [18] analyzed the natural convective flow and heat transfer features for a heated cylinder kept in a square enclosure with different thermal boundary conditions. Braga and Lemos [4] numerically studied steady laminar natural convection within a square cavity filled with a fixed amount of conducting solid material consisting of either circular or square obstacles. The authors showed that the average Nusselt number for cylindrical rods is slightly lower than those for square rods. Lee and Ha [10] investigated natural convection in a horizontal layer of fluid with a conducting body in the interior, using an accurate and efficient Chebyshev spectral collocation approach. Later on, the same authors Lee and Ha [11] also studied natural convection in horizontal layer of fluid with heat generating conducting body in the interior. Rahman et al. [17] studied effect of a heat conducting horizontal circular cylinder on mhd mixed convection in a lid-driven cavity along with joule heating. The objective of the present study have been investigated numerically with the effect of magneto-hydrodynamic (MHD) mixed convection flow in a lid-driven triangular cavity.

II. Model Specifications

The physical model considered here is shown in Fig.1, along with the important geometric parameters. The heat transfer and the fluid flow in a two-dimensional triangular cavity with a fluid whose left wall is subjected to cold temperature T_c (k) and moving with velocity V . The bottom wall of the cavity is subjected to hot temperature T_h (k) while the inclined wall is kept adiabatic. The fluid was assumed with Prandtl number ($Pr = 0.71-6.0$), Reynolds number ($Re = 40-100$) and Newtonian, and the fluid flow is considered to be laminar. The properties of the fluid were assumed to be constant.

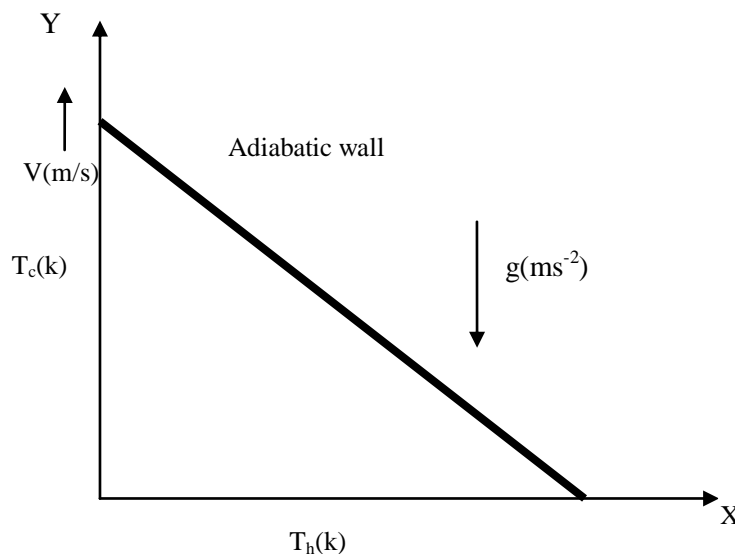


Figure-1. schematic diagram of the physical system

2.1 Mathematical Model

The fundamental laws used to solve the fluid flow and heat transfer problems are the conservation of mass (continuity equations), conservation of momentums (momentum equations), and conservation of energy (energy equations), which constitute a set of coupled, nonlinear, and partial differential equations. For laminar incompressible thermal flow, the buoyancy force is included here as a body force in the v -momentum equation. The governing equations for the two-dimensional steady flow are found after invoking the Boussinesq approximation and neglecting radiation and viscous dissipation. Using non-dimensional variables defined in the nomenclature, the non-dimensional governing equations (1) – (4) are obtained as follows:

Continuity equation

$$\frac{\partial U}{\partial X} + \frac{\partial V}{\partial Y} = 0 \tag{1}$$

Momentum equations

$$U \frac{\partial U}{\partial X} + V \frac{\partial U}{\partial Y} = -\frac{\partial P}{\partial X} + \frac{1}{Re} \left(\frac{\partial^2 U}{\partial X^2} + \frac{\partial^2 U}{\partial Y^2} \right) \tag{2}$$

$$U \frac{\partial V}{\partial X} + V \frac{\partial V}{\partial Y} = -\frac{\partial P}{\partial Y} + \frac{1}{Re} \left(\frac{\partial^2 V}{\partial X^2} + \frac{\partial^2 V}{\partial Y^2} \right) + Ra Pr \theta \tag{3}$$

Energy equation

$$U \frac{\partial \theta}{\partial X} + V \frac{\partial \theta}{\partial Y} = \frac{1}{Re Pr} \left(\frac{\partial^2 \theta}{\partial X^2} + \frac{\partial^2 \theta}{\partial Y^2} \right) \tag{4}$$

2.2 boundary conditions

The dimensionless boundary conditions under consideration can be written as:

At the vertical wall: $U = 0, V = 1, \theta = 0$

At the horizontal wall: $U = 0, V = 0, \theta = 1$

At the inclined wall: $U = 0, V = 0, \frac{\partial \theta}{\partial N} = 0$

Where N is the non-dimensional distances either along X or Y direction acting normal to the surface. The average Nusselt number at the heated wall of the cavity based on the non-dimensional variables may be

expressed as $Nu = - \int_0^1 \left(\frac{\partial \theta}{\partial Y} \right)_{y=0} dX$ and the bulk average temperature defined as $\theta_{av} = \int \theta d\bar{V} / \bar{V}$, where \bar{V} (m^3) is

the cavity volume.

The above equations were normalized using the following dimensionless scales:

$X = x/L, Y = y/L, U = u/v_0, V = v/v_0, Pr = \nu/\alpha, \Delta T = T_h - T_c,$

$Re = UL/\nu, Gr = \beta g \Delta T L^3 / \nu^2, \theta = (T - T_c) / (T_h - T_c)$

III. Numerical Analysis

The governing equations along with the boundary conditions are solved numerically by employing Galerkin weighted residual finite techniques. The application of this technique is well described by Taylor and Hood [19] and Dechaumphai [5, 6]. The finite element formulation and computational procedure have been omitted here for brevity.

IV. Grid Independence Test

Preliminary results are obtained to inspect the field variables grid independency solutions. Test for the accuracy of grid fineness has been carried out to find out the optimum grid number. In order to obtain grid independent solution, a grid refinement study is performed for a triangular cavity with $Pr = 0.71, Re = 50$ and $Ra = 10^4$. Fig.2 shows, the convergence of the average Nusselt number, Nu at the heated surface with grid refinement. It is observed that grid independence is achieved with 13967 elements where there is insignificant change in Nu with further increase of mesh elements. We believe that for this inconsequential change before the element 13967 should not be taken as for grid independence. In table 1, Six different non-uniform grids with the following number of nodes and elements were considered for the grid refinement tests: 9138 nodes, 1523 elements; 36102 nodes, 6017 elements; 49260 nodes, 8210 elements; 62280 nodes, 10380 elements; 83802 nodes, 13967 elements; 99192 nodes, 16532 elements. From these values, 83802 nodes, 13967 elements can be

chosen throughout the simulation to optimize the relation between the accuracy required and the computing time.

Table 1: Grid Sensitivity Check at $Pr = 0.71$, $Re = 50$ and $Ra = 10^4$.

Nodes (elements)	9138 (1523)	36102 (6017)	49260 (8210)	62280 (10380)	83802 (13967)	99192 (16532)
Nu	2.4095029	2.5207933	2.5207523	2.6746807	2.7484171	2.75818
Time(s)	8.297	34.0	47.703	67.297	94.828	112.25

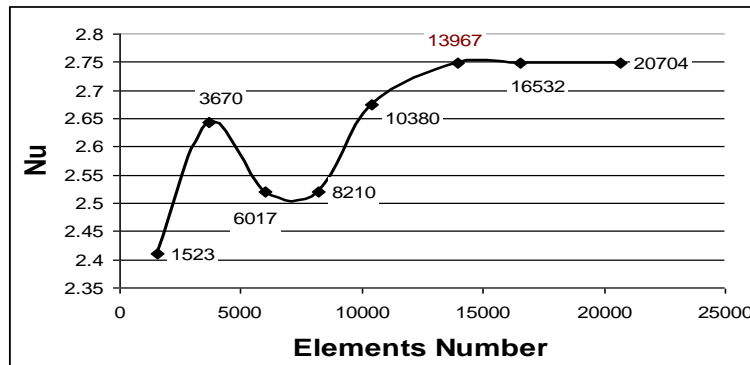


Figure-2: convergence of average nusselt number with grid refinement for $Pr = 0.71$, $Re = 40$ and $Ra = 10^4$.

V. Result and Discussion

Numerical results are presented in order to conclude the properties of the presence of dimensionless parameters in lid-driven triangular cavity with a heat conducting horizontal bottom wall and the adiabatic inclined wall. The left wall of the cavity is kept at cooled temperature T_c (k) which is moving with V (m/s) vertically.

Two-dimensional forms of Navier-Stokes equations along with the energy equations have been solved using Galerkin finite element method. The dimensionless parameters that must be specified for the system are Reynolds number Re , Rayleigh number Ra , and Prandtl number Pr . Since so many basic dimensionless parameters are required to characterize a system, an analysis of all combinations of these parameters is not practical. The numerical results will be aimed to explain the effect of several parameters at a small fraction of the possible situations by simplifying the configuration. Results are obtained for a range of Rayleigh number from 10^3 to 10^4 at $Pr = 0.71$ - 6.0 and $Re = 40$ -100, with constant physical properties. The parametric studies for a wide range of governing parameters show consistent performance of the present numerical approach to obtain as stream functions and temperature profiles. The computational results indicate that the heat transfer coefficient is strongly affected by Rayleigh number. Representative distributions of average Nusselt number at the heated surface and average bulk temperature of the fluid in the cavity will then be presented.

The results were compared with those reported by Basak et al.[3], obtained with an extended computational domain. In Table 2, a comparison between the average Nusselt numbers is presented. The results from the present experiment are almost the same as Basak et.al.

Table 2: Comparison of The Results For The Constant Surface Temperature With $Pr = 0.71$

Ra	Nu_{av}	
	Present work	Basak et al.[3]
10^3	5.49	5.40
10^4	5.77	5.56
10^5	7.08	7.54

5.1 Effects of Reynolds Number (Re)

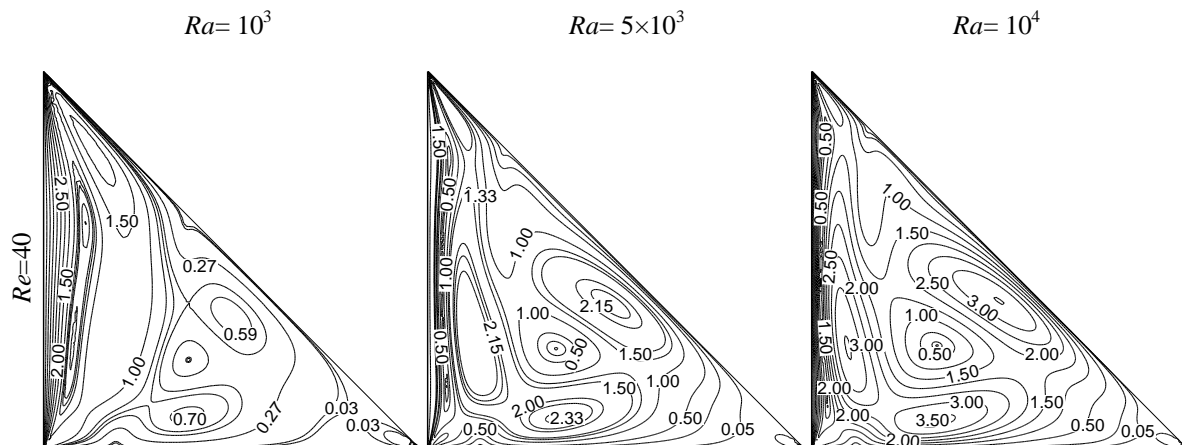
The fluid flow patterns inside the cavity are presented in terms of streamlines and isotherms in the figs. 3-4 at the range of Reynolds number Re ($Re = 40$ -100) and $Ra = 10^3$ - 10^4 while $Pr = 0.71$. Using the definition of stream function (ψ), the streamlines with 'positive numerical value' corresponds to anti-clockwise circulation, and those with 'negative numerical value' correspond to clockwise circulation. As expected due to the upward motion of the bottom wall, fluid rise up along the side of the cold vertical wall and flow down along the right vertical wall forming a roll with anti-clockwise rotation inside the cavity for the different values of Ra at $Re = 40$. It is also observed that the orientation of the core in the recirculation cell changes as Reynolds number Re

changes. Next at $Re = 50$, secondary rotating cells are developed in the cavity for all values of Ra , which indicates both the conducting force and buoyant force are present in the cavity. In this fig. at low $Ra = 10^3$, the 'positive numerical value' of stream function is low in the cell, which is due to conductive force occupying most of the part of the cavity and other two secondary rotating cells due to development buoyant force at the bottom and inclined wall. However, as Ra increases the value of ψ and the cells become larger in size. It is also seen from figure 3 that value of ψ of the anticlockwise rotating cell increases sharply and more tightened to the neighboring boundary wall, indicating a sign of supremacy of free convection in the cavity at $Re = 100$ and different Ra .

Now we draw the attention to see the effect of increasing Reynolds number Re on the temperature distribution in the cavity. From the fig.4, it can be seen that isothermal lines are nearly parallel to the hot wall at $Re = 40$ and $Ra = 10^3$, which is similar to conduction-like distribution. It is also seen that isothermal lines start to turn back from the cold wall to the hot wall near the bottom wall at $Ra = 5 \times 10^3$ and $Re = 40$, due to the dominating influence of conduction and forced convection in the lower part of the cavity. More significant distortion in isothermal lines near the left bottom corner of the cavity is observed at the higher values of Ra . The isotherm patterns reflect a conductive pattern of energy transfer at the lower values of Re ($Re = 40, 50$) and a convective pattern of energy transfer at the higher values of Re ($Re = 70, 100$). On the other hand, the convective distortion of isothermal lines start to appear at $Ra = 5 \times 10^3$ and $Re = 10^3$. At $Ra = 5 \times 10^3$ and $Re = 70$, it is seen that the isothermal lines turn back towards the left cold wall near the top of the cavity and a thermal boundary layer is developed near the left vertical (cold) wall due to the dominating influence of the convective current in the upper part of the cavity. Finally at $Ra = 10^4$, the convective distortion in the isotherms become more and the thermal boundary layer near the cold wall becomes more concentrated with further increasing the values of Reynolds number due to the strong influence of the convective current.

The effect of Reynolds number on average Nusselt number (Nu) at the heated bottom wall and average fluid temperature (θ_{av}) in the cavity are displayed as a function of Rayleigh number at some particular Reynolds number in figs.5 & 6 for the above mentioned cavity. It is observed that the average Nusselt number at the hot wall increases considerably in the forced convection dominated region and increases very penetratingly in the free convection dominated region with increasing Ra for the higher values of Reynolds number Re ($Re = 50, 70$ and 100). However, maximum values of Nu is found for the highest value of Re ($Re = 100$) at free convection dominated region. On the other hand, the average fluid temperature (θ_{av}) in the cavity increases gradually for higher values of Re ($Re = 50, 70, 100$) and but suddenly fall dramatically for the all values of Re with increasing Ra . In addition, the values of θ_{av} are found minimum for $Re = 40$ at $Ra = 10^4$, at free convection dominated region.

Fig.6 displays the variation of the average bulk temperature against the Rayleigh number for various Reynolds numbers. The average temperature decreases smoothly with increase of Ra . It is an interesting observation that at lower Re , the average bulk temperature is affected by Rayleigh number.



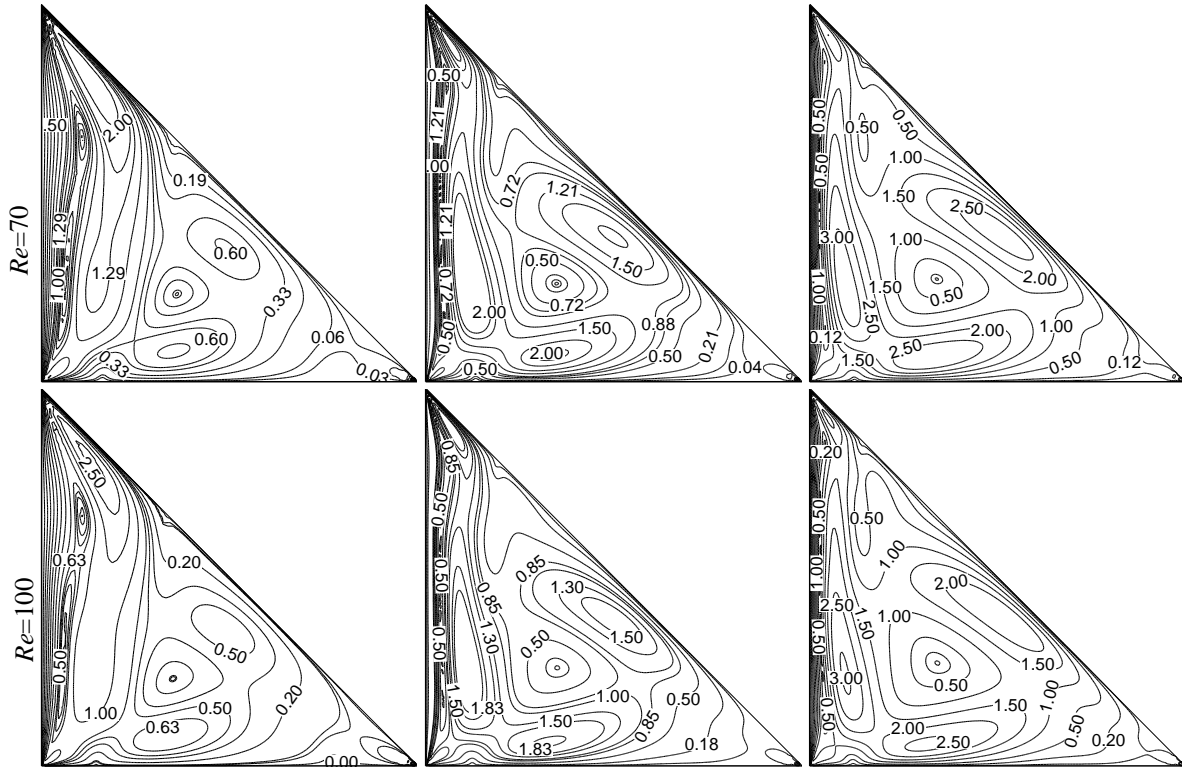
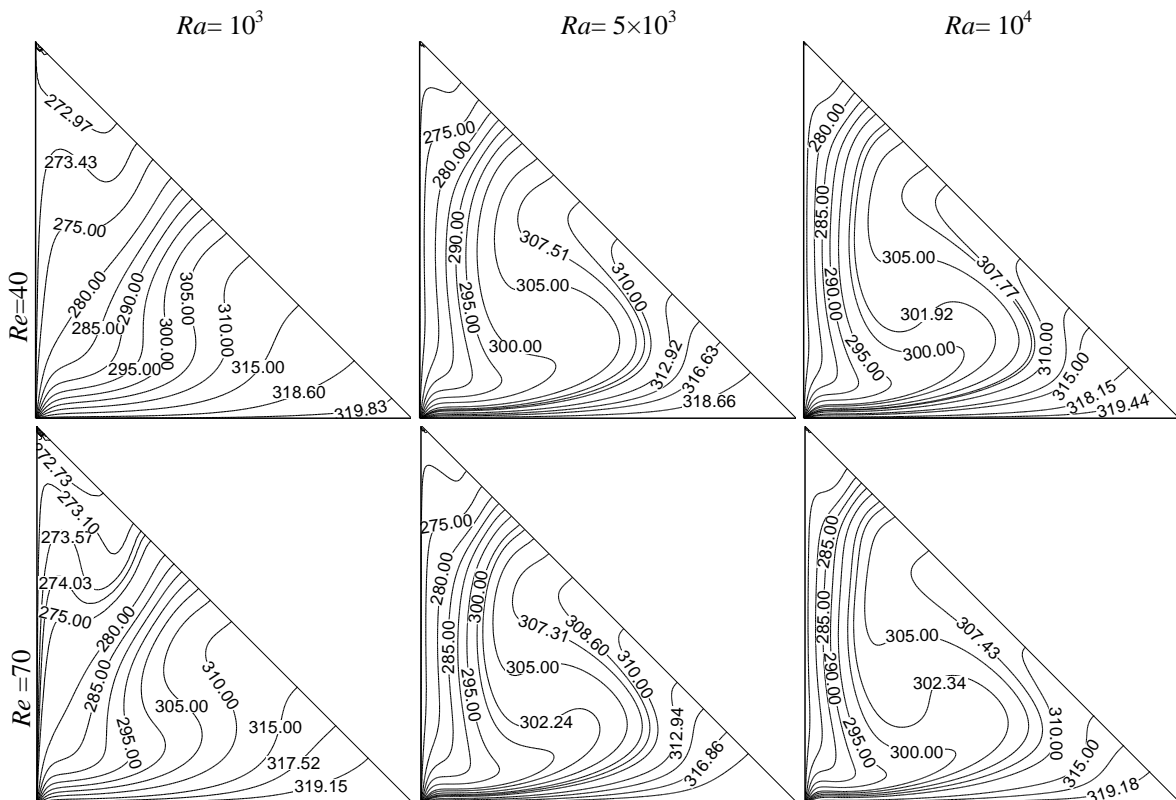


Figure-3: Streamlines patterns for different Re (40, 70, 100) when $Pr = 0.71$.



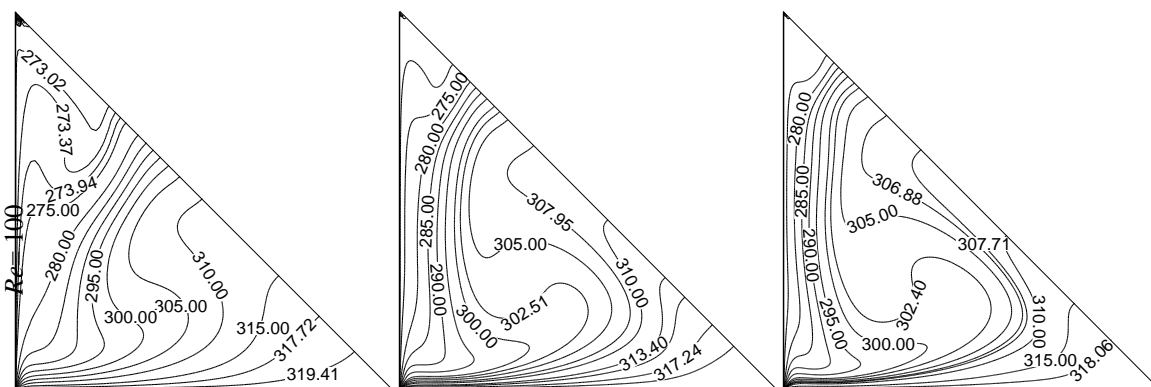


Figure-4: Isotherms patterns for different Re (40, 70,100) when $Pr = 0.71$.

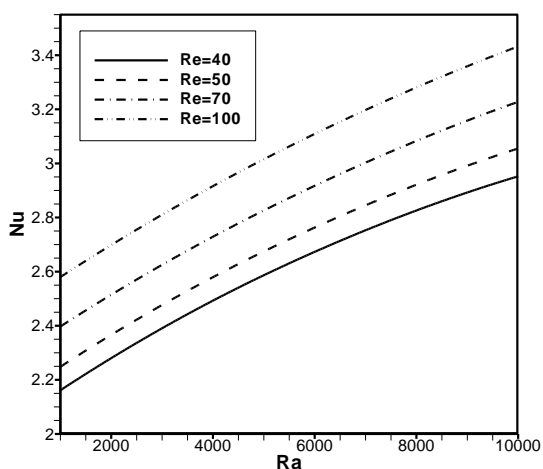


Figure-5: effect of average nusselt number and rayleigh number while $Pr = 0.71$.

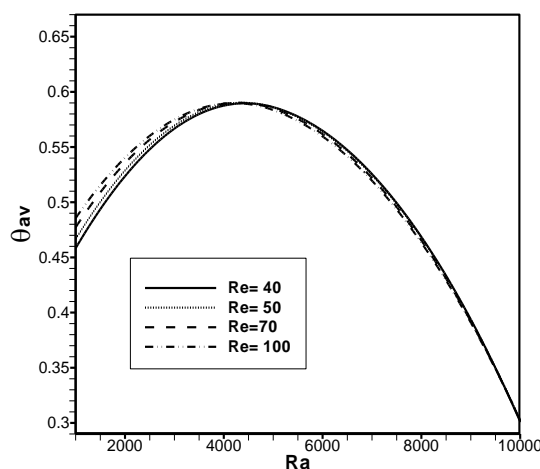


Figure-6: effect of average bulk temperature and rayleigh number while $Pr = 0.71$.

5.2 Effects of Prandtl Number (Pr)

Figs.7–8 display the effects of Ra (10^3 – 10^4) and Pr (0.71–6.0) while the bottom wall is heated and the left moving wall is maintained at cold temperature. The fluid near the hot (bottom) wall is of lower density, so it moves upward while the relatively heavy fluid near cold (left) wall moves downward and this fluid is heated up. Thus the fluid motion completes the circulation. As mentioned before by the definition of stream function (ψ), the positive number of the streamlines corresponds to anti-clockwise circulation, and those with negative number corresponds to clockwise circulation in the cavity. Note that, for steady flow, streamlines are equivalent to the paths followed by the individual particles in the fluid. Results indicate that at low Rayleigh number ($Ra = 10^3$), the isotherm lines are smooth and monotonic as shown for $Pr = 0.71$ in Figure 7. The magnitudes of the stream function are very small. This illustrates that at low Ra the flow is mostly due to conduction.

At $Ra = 5 \times 10^3$ and $Pr = 0.71$, the circulations near the central regime are stronger and consequently the thermal boundary layer starts getting shifted towards the left wall (fig.7).The presence of significant convection is also exhibited in the temperature profile which gets pushed towards the upper portion of left wall. As Rayleigh number increases to 10^4 , the buoyancy driven circulation inside the cavity is also increased as seen from a greater magnitudes of the stream function (fig.8). From the fig.8 for $Pr = 6.0$, it shows the circulations are bigger near the center due to convection and least at the vicinity wall due to no-slip boundary conditions. The greater circulation in central regime follows a progressive packaging around the center of rotation, and a more and more pronounced compression of the isotherms towards the bottom and left corner of triangular cavity occurs. Due to high circulations, the temperature contours with 300.00 condensed in a very small regime at the bottom wall and this may cause bigger heat transfer rates at the bottom wall. It may also be distinguished that the higher circulation pushes fluid near the upper region of the left wall, and the fluid is pulled away from the central region of the left wall. Consequently, at $Ra = 10^4$, the temperature gradients near the bottom wall are found to be significantly high.

The effects of Prandtl number on average Nusselt number Nu at the heated surface and average bulk temperature (θ_{av}) in the cavity is illustrated at figs.9 & 10 with $Re = 50$. From these figs., it is found that the average Nusselt number Nu moves up calmly with increasing Pr . Moreover, it is also to be highlighted that the

highest heat transfer rate occurs for the highest values of Pr ($= 6.0$). This is because, the fluid with $Pr = 7.0$ has a lower thermal diffusivity than that of the fluid with $Pr = 0.72$. On the other hand, the average bulk temperature (θ_{av}) of the fluid in the cavity increases very sharply in forced dominated region inside the cavity and reached to the highest bulk temperature rate at $Pr=0.71$. But in the free dominated region bulk temperature rate is slower for the higher values of Pr .

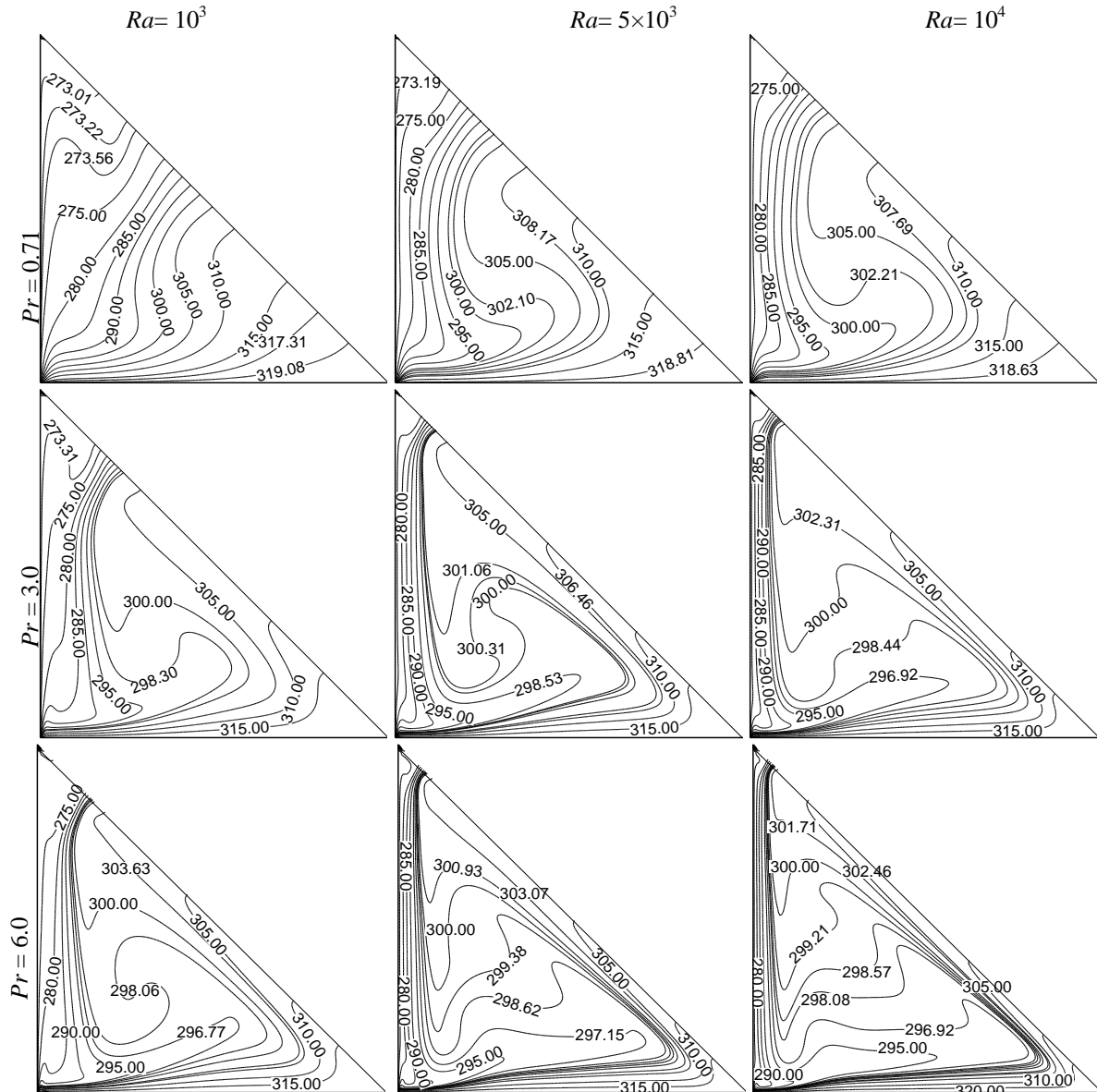


Figure-7: Isotherms patterns for different Pr (0.71, 3.0, 6.0) when $Re = 40$.

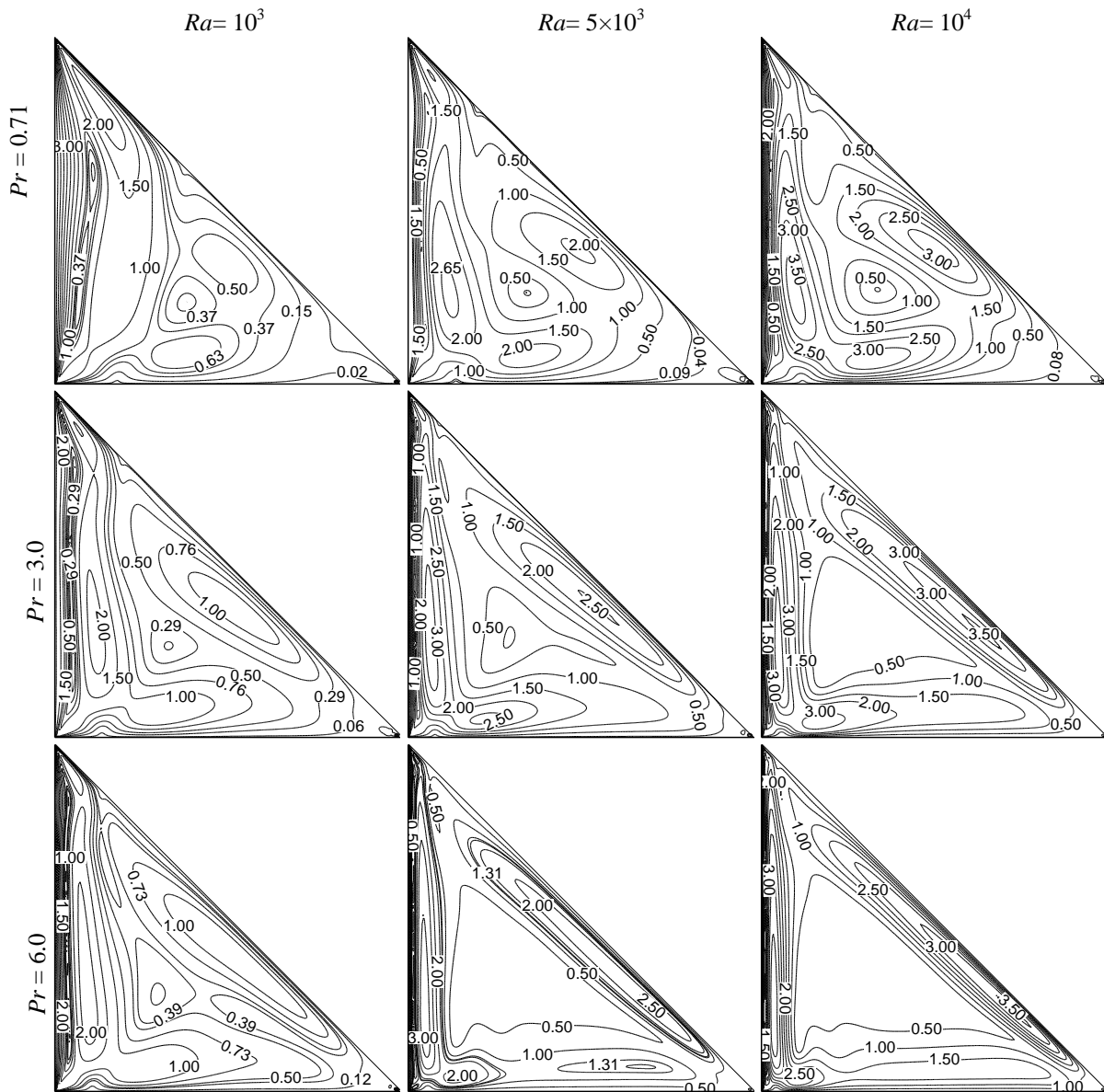


Figure-8: streamline patterns for different Pr (0.71, 3.0, 6.0) when $Re = 40$.

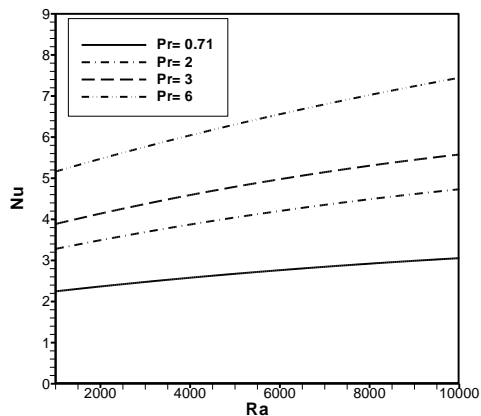


Figure-9: effect of average nusselt number and rayleigh number while $Re = 40$

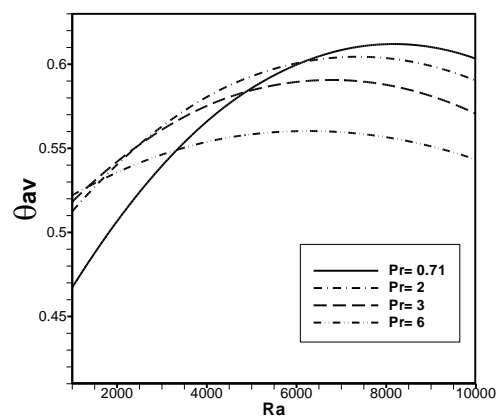


Figure-10: effect of average bulk temperature and rayleigh number while $Re = 40$.

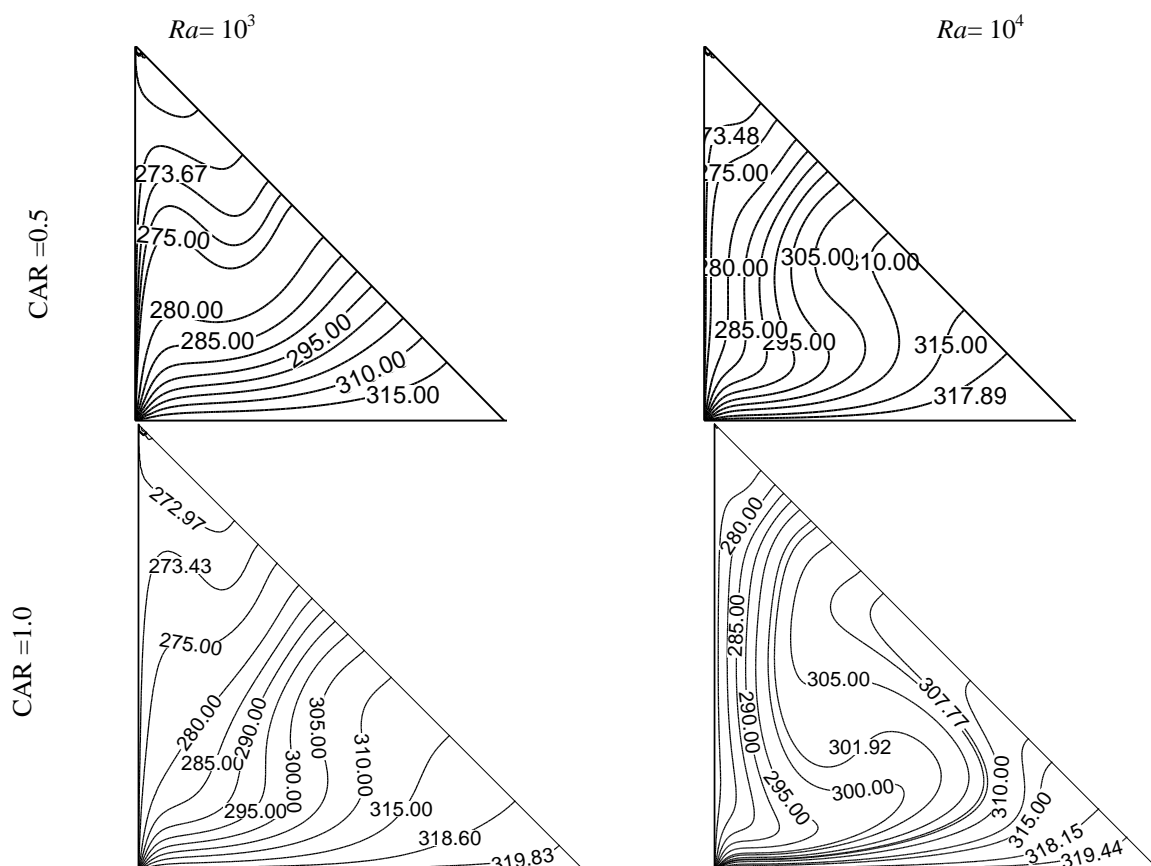
5.3 Effect of cavity aspect ratio (CAR)

In order to investigate the convective heat transfer behavior at other aspect ratios, computations have also been done for three additional cavity aspect ratios of 0.5, 1.0 and 1.5, while keeping $Re = 50$, and $Pr = 0.71$. The flow patterns and temperature fields for $CAR = 0.5, 1.0$, and 1.5 have been compared in Figs.11 and 12.

From the fig.11, it has been seen that isothermal lines are nearly parallel to the hot wall at $Re = 50$ and $Pr = 0.71$, which is similar to conduction-like distribution. It is also seen that isothermal lines start to turn back from the hot wall to the cold wall near the bottom wall at $Ra = 5 \times 10^3$ (disappear in paper) and $Re = 50$ due to the dominating influence of conduction and forced convection in the lower part of the cavity. More significant distortion in isothermal lines near the left bottom corner of the cavity is observed at the higher values of Ra .

At $Ra = 10^3$, it has been seen that isotherm lines are nearly linear and occupy most of the part of the cavity for the case of $CAR = 0.5$, the isothermal lines becomes non-linear and concentrated near the hot wall in the cavity with the increasing values of CAR , because of the distance between the hot wall and the cold wall. In particular the isotherm line 315.00 is near the hot wall but it is away from the hot wall with increase of CAR . The isotherm lines are more distorted for $Ra = 5 \times 10^3$ and 10^4 , and become more dense with heated wall with increase of CAR from 0.5 to 1.5. As a result, thermal boundary layer concentrated with cold wall due to strong convective flow. In the case of stream line, some recirculation cells have developed in the cavity. This recirculation cell gradually increases with the increase of the value of CAR , due to increasing the available space for the fluid in the cavity. It is also observed that secondary rotating cells are developed in the cavity for all values of Ra , which indicates both the conducting force and buoyant force are present in the cavity.

The average Nusselt number (Nu) at the heated source and the average bulk temperature (θ_{av}) of the fluid in the cavity for $CAR = 0.5, 1.0$ and 1.5 have been shown in fig.13. The average Nusselt number and average temperature of the fluid at the hot wall is increased with increasing values of CAR . This is because of the increase of space in the cavity. The maximum value of Nu is found for the $CAR = 1.5$ at free convection dominated region but the average fluid temperature (θ_{av}) in the cavity increases gradually with respect to CAR .



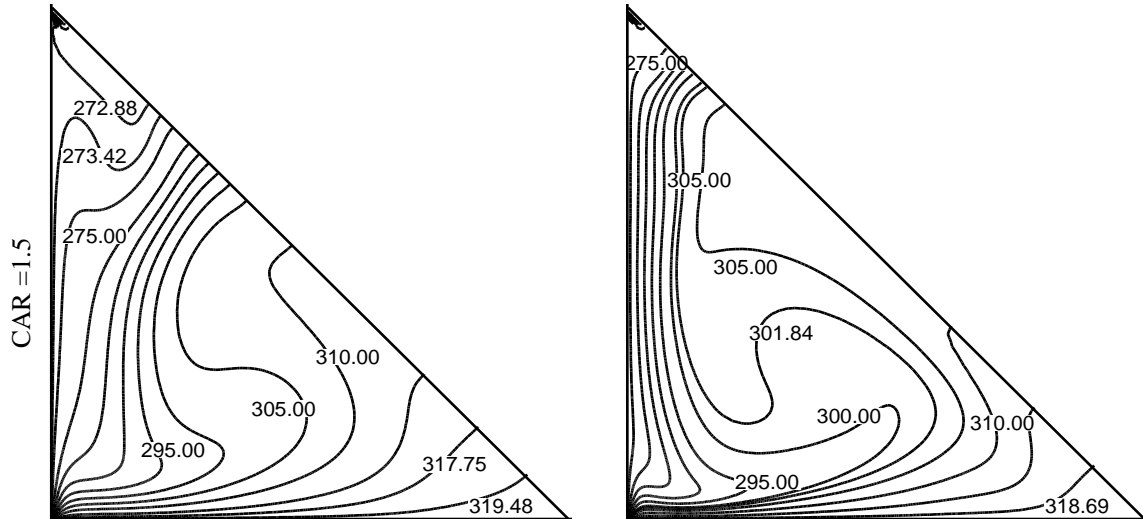
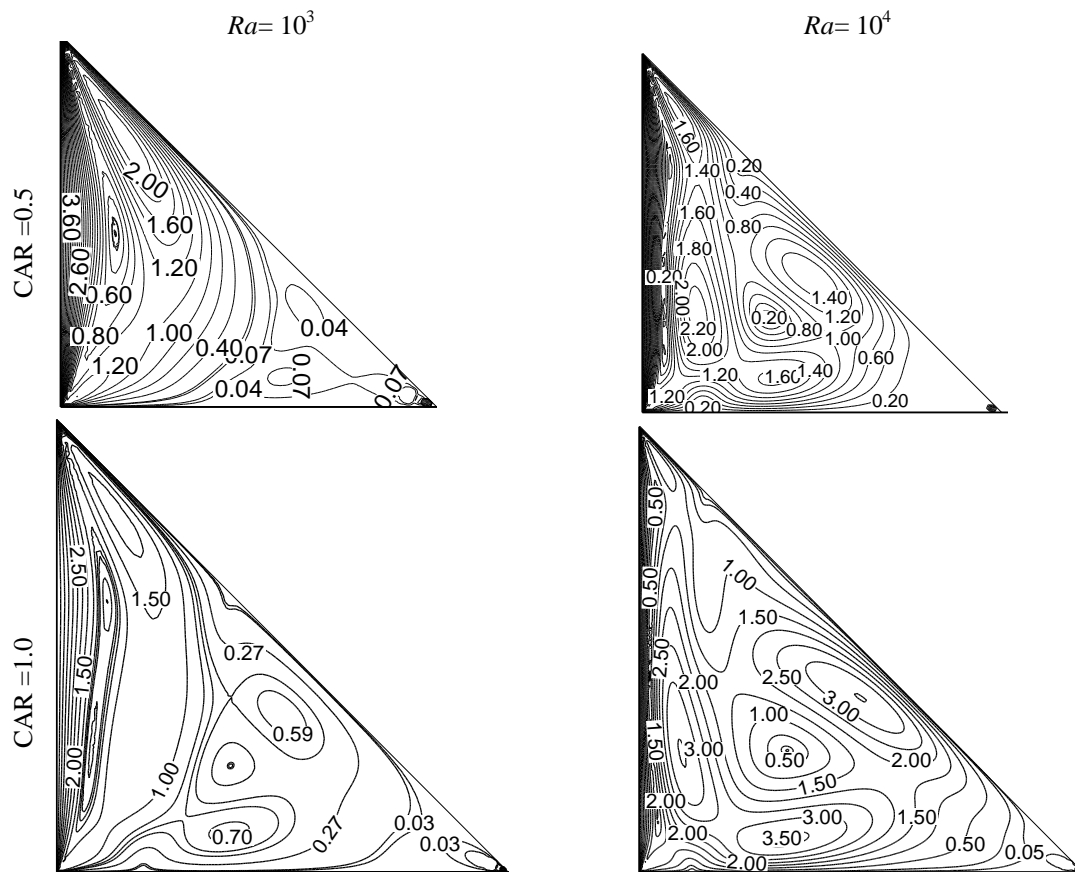


Figure-11: Isotherms patterns for different CAR (0.5, 1.0, 1.5) when $Pr = 0.71$ and $Re=40$.



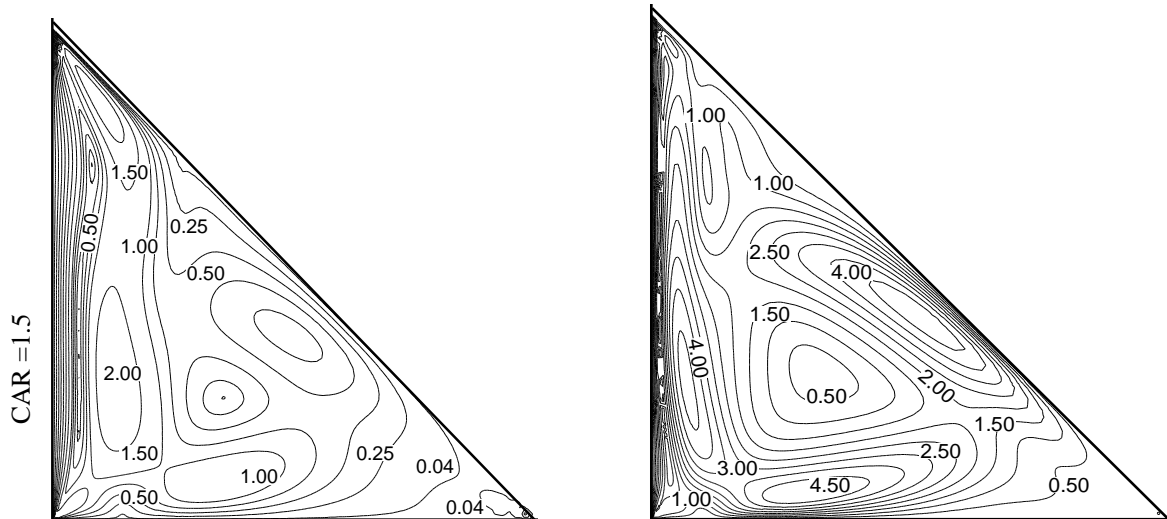


Figure-12: Stream line patterns for different CAR (0.5, 1.0, 1.5) when $Pr = 0.71$ and $Re=40$

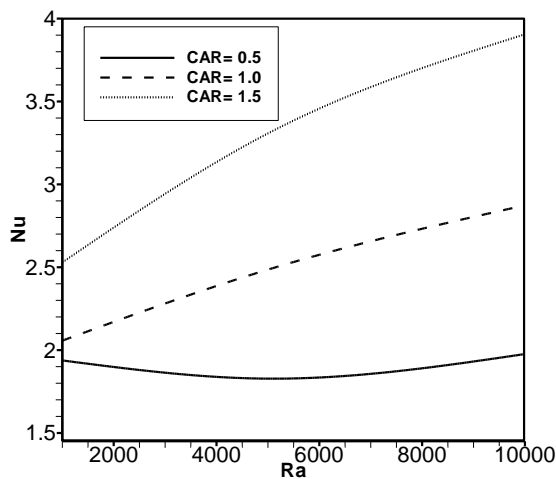


Figure-13: Effect of average Nusselt number and Rayleigh number while $Re = 40$

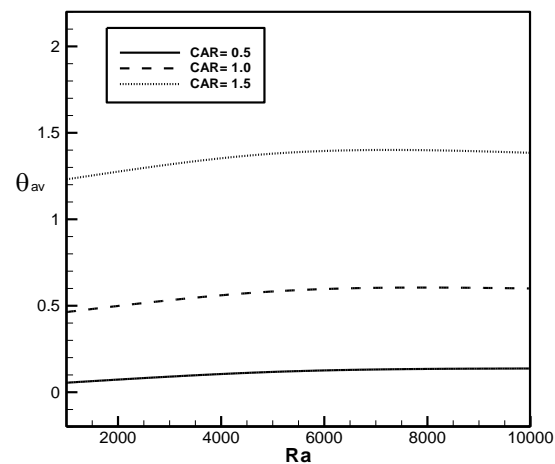


Figure-14: Effect of average bulk temperature and Rayleigh number while $Re = 40$.

VI. Conclusion

A finite element method for steady-state incompressible conjugate effect of mixed convection and conduction has been presented. The finite element equations were derived from the governing flow equations that consist of the conservation of mass, momentum, and energy equations. The derived finite element equations are nonlinear requiring an iterative technique solver. The Galerkin weighted residual method is applied to solve these nonlinear equations for solutions of the nodal velocity components, temperatures, and pressures. The above example demonstrates the capability of the finite element formulation that can provide insight to steady-state incompressible conjugate effect of mixed convection and conduction problem. The investigation is carried out for a number of relevant dimensionless groups, namely Rayleigh number Ra , Hartmann number Ha , Reynolds number Re , and Prandtl numbers Pr . From an examination of heat transfer and fluid flow phenomena revealed by the numerical experiments, the following major conclusions have been drawn:

- Interesting behavior of the flow and thermal fields with varying Reynolds number is observed. In addition, the numerical solutions indicate that the increasing values of Re leads to higher heat transfer rate from the heat source but other side the average bulk temperature decline significantly.
- As Ra escalates the value of the magnitude of the stream function is ψ and the cells become larger in size, become more attested to the boundary wall.
- The impact of Prandtl number on the flow and thermal fields in the cavity is found to be more pronounced, if Re is kept fixed. The maximum heat transfer is experimented at the highest value of Pr for the considered value of Ra .

- The average bulk temperature is high for $Pr = 0.71$ in free convection region.
- Thermal boundary layer thickness is thinner for increasing of Rayleigh number because slowly the conductive heat transfer turns into convective heat transfer.
- Various vortices entering into the flow field and a secondary vortex at the inclined and bottom wall of the cavity is seen in the streamlines.

Acknowledgements

Authors would like to thank the Department of Mathematics, Bangladesh University of Business & Technology (BUBT), for providing computer facility during this work. We also express our gratitude to anonymous reviewers for their suggestions which improved the quality of the manuscript.

References

- [1]. Akinsete V.A., Coleman T.A., Heat transfer by steady laminar free convection in triangular enclosures, *International Journal of Heat and Mass Transfer*, 25(7), 1982, 991–998.
- [2]. Aydin, O., Yang, W. J., Mixed convection in cavities with a locally heated lower wall and moving side walls, *Numer. Heat Transfer*, 37(7), 2000, 695-710.
- [3]. Basak T., Roy S., Krishna Babu S., Balakrishnan A.R., Finite element analysis of natural convection flow in a isosceles triangular enclosure due to uniform and non-uniform heating at the side walls, *International Journal of Heat Mass Transfer*, 51(17), 2008, 4496–4505.
- [4]. Braga, E. J., de Lemos, M. J. S., Laminar natural convection in cavities filed with circular and square rods, *Int. Commun. in Heat and Mass Transfer*, 32(10),2005, 1289-1297.
- [5]. Dechaumphai, P., Adaptive finite element technique for heat transfer problems, *Energy, Heat & Mass transfer*, 17(2) .1995, 87-94.
- [6]. Dechaumphai, P., *Finite Element Method in Engineering* (Bangkok, Chulalongkorn University Press, 1999)
- [7]. Hossain, M. A., Gorla, R. S. R., Effect of viscous dissipation on mixed convection flow of water near its density maximum in a rectangular enclosure with isothermal wall, *Int. J. of Numer. Methods for Heat and Fluid Flow* 16 (1), 2006, 5-17.
- [8]. Karyakin YU.E, Sokovishin YU.A., Transient natural convection in triangular enclosures, *International Journal of Heat and Mass Transfer*, 31(9), 1988, 1759–1766.
- [9]. Lee, J. R., Ha, M. Y., A numerical study of natural convection in a horizontal enclosure with a conducting body, *Int. J. of Heat and Mass Transfer*, 48(16),2005, 3308-3318.
- [10]. Lee, J. R., Ha, M. Y., Numerical simulation of natural convection in a horizontal enclosure with a heat-generating conducting body, *Int. J. of Heat and Mass Transfer*, 49(15-16), 2006, 2684-2702.
- [11]. Luo, W. J., Yang, R. J., Multiple fluid flow and heat transfer solutions in a two-sided lid-driven cavity, *Int. J. of Heat and Mass Transfer*, 50(11-12),2007, 2394-2405.
- [12]. Li M., Tang T., *Steady viscous flow in a triangular cavity by efficient numerical techniques*, *Comput. Math. Appl.*,31 (1),1996, 55-65.
- [13]. Moallemi, M. K., Jang, K. S., Prandtl number effects on laminar mixed convection heat transfer in a lid-driven cavity, *Int. J. Heat and Mass Transfer*, 35(8),1992,1881-1892.
- [14]. Oztop, H. F., Dagtekin, I., Mixed convection in two-sided lid-driven differentially heated square cavity, *Int. J. of Heat and Mass Transfer*, 47(8-9),2004, 1761-1769.
- [15]. Prasad, A. K., Koseff, J. R., 1996. Combined forced and natural convection heat transfer in a deep lid-driven cavity flow, *Int. J. Heat and Fluid Flow* 17(5),1996, 460-467.
- [16]. Rahman, M.M., Mamun M.A.H., Saidur, R., and Nagata Shuichi, Effect Of a Heat Conducting Horizontal Circular Cylinder on MHD Mixed Convection In A Lid- Driven Cavity Along With Joule Heating, *Int. J. of Mechanical and Materials Eng. (IJMME)*, 4 (3), 2009, 256-265.
- [17]. Roychowdhury, D.G, Das, S.K., Sundararajan, T.S., 2002, Numerical simulation of natural convection heat transfer and fluid flow around a heated cylinder inside an enclosure, *Heat and Mass Transfer*, 38(7-8), 2002, 565-576.
- [18]. Taylor,C., Hood,P., A Numerical Solution of the Navier-Stokes Equations Using Finite Element technique, *Computer and Fluids* 1, 73 (1973). doi:10.1016/0045-7930(73)90027-3